J Mol Model (2010) 16:1011–1020
DOI 10.1007/s00894-009-0611-1

ORIGINAL PAPER

Effect of pathogenic mutations on the structure and dynamics of Alzheimer's $A\beta_{42}$-amyloid oligomers

Kristin Kassler · Anselm H. C. Horn · Heinrich Sticht

Received: 17 August 2009 / Accepted: 1 October 2009 / Published online: 12 November 2009

Abstract Converging lines of evidence suggest that soluble Aβ-amyloid oligomers play a pivotal role in the pathogenesis of Alzheimer's disease, and present direct effectors of synaptic and cognitive dysfunction. Three pathological E22-Aβ-amyloid point mutants (E22G, E22K, E22Q) and the deletion mutant E22Δ exhibit an enhanced tendency to form prefibrillar aggregates. The present study assessed the effect of these four mutations using molecular dynamics simulations and subsequent structural and energetic analyses. Our data shows that E22 plays a unique role in wild type Aβ, since it has a destabilising effect on the oligomer structure due to electrostatic repulsion between adjacent E22 side chains. Mutations in which E22 is replaced by an uncharged residue result in higher oligomer stability. This effect is also observed to a lesser extent for the E22K mutation and is consistent with its lower pathogenicity compared to other mutants. Interestingly, deletion of E22 does not destroy the amyloid fold but is compensated by local changes in the backbone geometry that allow the preservation of a structurally important salt bridge. The finding that all mutant oligomers investigated exhibit higher internal stability than the wild type offers an explanation for the experimentally observed enhanced oligomer formation and stability.

Keywords Molecular dynamics · Energetic analysis · Protein interaction · Oligomerisation · Fibrillation · Glutamate 22

K. Kassler · A. H. C. Horn · H. Sticht (✉)
Bioinformatik, Institut für Biochemie,
Friedrich-Alexander-Universität Erlangen-Nürnberg,
Fahrstraße 17,
91054 Erlangen, Germany
e-mail: H.Sticht@biochem.uni-erlangen.de

Introduction

When the physician Alois Alzheimer spotted a rare case of progressive dementia in 1906 [1], he could not presage that 100 years later that disease would be one of the most severe health problems of the world's industrial nations. Persons with Alzheimer's disease (AD) suffer from a progressive decline of memory and cognition, resulting from the dysfunction or loss of neurons [2, 3]. One of the most prominent cytopathological hallmarks of AD-affected tissue is a growing number of fibrillar plaques composed of abnormally altered and aggregated Aβ-amyloid protein, which is a cleavage product of amyloid precursor protein (APP) [4]. Although two pathological Aβ-amyloid isoforms, $A\beta_{42}$ and $A\beta_{40}$, are known, the 42-amino-acid-long peptide appears to be the more disease-relevant species [5]. The deposition of Aβ-fibrils into plaques is preceded by an aggregation pathway involving several intermediate states such as oligomers and protofibrils [6].

Important insights into Aβ aggregation came from the structures of $A\beta_{40}$ [7, 8] and $A\beta_{42}$ [9] in the fibril state as determined by NMR techniques. For the monomeric subunits, both structures consistently reveal two β-strands connected by a turn, thus forming a U-shaped topology [8–10]. The monomeric subunits form a longitudinal stack, thereby creating two parallel in-register β-sheets (Fig. 1a). Key features of Aβ-fibril stability are the intermolecular salt bridges between D23 of the i^{th} and K28 of the $(i+1)^{th}$ Aβ monomer and the inter-sheet side chain packing interactions between hydrophobic residues of the i^{th} and its two adjacent layers ($i-1$, $i+1$), thus forming a cross β-structure. Amyloid growth can proceed longitudinally, i.e. the adsorption of new monomers along the fibril axis (Fig. 1a), and laterally, i.e. the association of another stack of monomers at the lateral surface of the growing aggregate

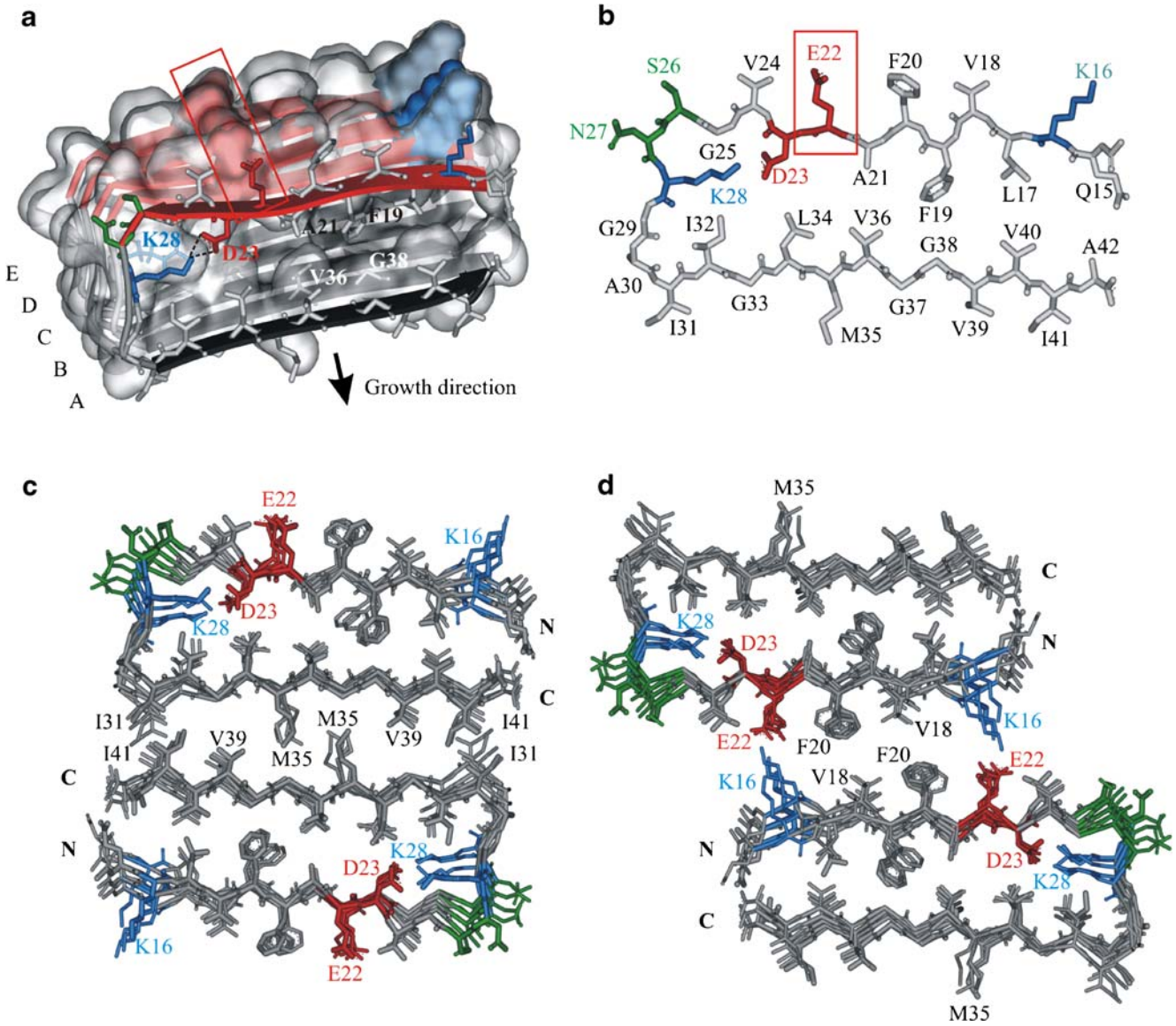

Fig. 1 **a** Schematic representation of the $A\beta_{42}$-amyloid pentamer structure used in the present study. The pentamer is composed of chains *A*–*E*. The two parallel in-register β-sheets are highlighted: sheet β1 (*red*) and sheet β2 (*black*). The pentamer is stabilised by intermolecular D23–K28 salt bridges, exemplified by the first salt bridge between D23 of chain *A* and K28 of chain *B*, and hydrophobic inter-sheet packing interactions, exemplified for the packing of residues A21 and F19 of chain *A* with V36 and G38 of chain *B*. An *arrow* indicates the direction of longitudinal growth. Negatively charged, positively charged, polar, and hydrophobic residues are coloured *red*, *blue*, *green*, and *grey*, respectively. The key residue E22 is indicated with a *red box*. **b** (β1-strand)-loop-(β2-strand) motif of a monomeric subunit showing the side chain orientation of residues 15–42 in detail. **c**, **d** Structural model of double-layered $A\beta_{42}$-pentamers illustrating the principles of fibril formation via lateral association. Lateral association might proceed either via the N-terminal strand β1 (**d**) or the C-terminal strand β2 (**c**) thus resulting in the so-called NN- or CC-interface

[8–15]. Lateral association might occur either via the N-terminal or via the C-terminal β-sheet, resulting in the so-called NN-interface (Fig. 1d) or the CC-interface (Fig. 1c).

While the extracellular fibrillar plaque deposition was originally assumed to be the disease initiating event [16, 17], today increasing evidence suggests that small soluble oligomers are the direct effectors of synaptic and cognitive dysfunction in AD [18, 19]. Moreover, it is even speculated that fibrillar plaques are rather neuroprotective [20]. The novel theory is supported by the discovery of pathological E22-Aβ-amyloid point mutants that are characterised by both an accelerated formation of Aβ-intermediate states and an enhanced amyloid neurotoxicity but less fibril formation [21, 22]. Aggregation properties, neurotoxicity and pathology of the Arctic (E22G), Italian (E22K), and Dutch (E22Q) variants are summarised in Table 1. The E22Δ variant, which was discovered recently in Japan, exhibits an enhanced aggregation rate compared to the wild type and is

Table 1 Aggregation properties (rate of aggregation, neurotoxicity and pathology) of disease associated E22-Aβ mutants compared to wild type. *AD* Alzheimer's disease, *CAA* Cerebral amyloid angiopathy

	Rate	Morphology	Neurotoxicity	Pathology
E22G (Arctic) [22, 46]	Accelerated	Small protofibrils and oligomers	Enhanced	AD dementia
E22K (Italian) [21]	Accelerated	Less fibrillar	Enhanced	CAA
E22Q (Dutch) [21, 52]	Accelerated	Rather amorphous than fibrillar; oligomers	Enhanced	CAA
E22Δ (Japanese) [23]	Accelerated	Small soluble oligomers, lack of fibrils	Enhanced	AD dementia

characterised by a strong enrichment of small soluble oligomers that are highly resistant to proteolytic digestion [23]. Finally, an E22 deletion was found to inhibit long-term potentiation more efficiently, and to induce synaptic alterations more potently than wild type Aβ-amyloid [24]. These findings demonstrate that not only mutation but also deletion of residue E22 leads to pathogenic effects.

While the E22Δ variant is as yet completely uncharacterised from a structural point of view, there exist several computational studies that aimed to characterise the molecular effects underlying increased aggregate formation by Aβ point mutants. Most studies have focussed either on the initial nucleation step leading to oligomers [12, 25], or on the lateral association step that is relevant for the formation of the fibril quaternary structure [13]. The effect of mutations E22G, E22Q, and E22K on Aβ-nucleation has been investigated by Krone et al. [25] using the Aβ (21–30) segment as a model system. From their work, these authors conclude that substitutions at E22 do little to alter the overall structure of the monomeric fragment, and that E22 might rather affect long-range interactions outside the monomeric structure [25]. The effect of E22 mutation on the formation of the $A\beta_{42}$-association was studied by Zheng et al. [13]. Mutation was found to hamper formation of the NN-interface (Fig. 1d), in which an E22–K16 bridge is formed between adjacent stacks of the protofibril. These findings suggest that the enrichment of oligomers results mainly from the inability of mutant oligomers to become incorporated into fibrils. The experimental data, however, show that mutant oligomers are not only enriched but also exhibit increased stability, e.g. resistance to proteolytic degradation, and a higher aggregation rate [23, 24]. This observation indicates the existence of additional structural properties that lead to increased internal stability of mutant Aβ-oligomers.

To address this point, the present work investigated the structure, dynamics and energetics of wild type and mutant Aβ-pentamers, including the structurally as yet completely uncharacterised deletion mutant E22Δ. For this purpose, molecular dynamics (MD) simulations were performed for the different systems. The significant differences detected in the internal stability of wild type and mutant pentamers are likely to play a key role in the pathogenicity of these mutants.

Materials and methods

Preparation of starting structures

All models and simulations are based on the $A\beta_{17–42}$ pentamer structure that was obtained from NMR-spectroscopic data (PDB entry 2BEG; model 10) [9]. Residues 15–16 were added to the model in an extended conformation to ensure the β-sheet complementarity of the U-shaped pentamer and to account for the secondary structure in the fibrillar form [26, 27]. Point mutants were generated starting from the elongated version of the wild type pentamer using SYBYL7.3 [28]. The side chain of E22 was replaced in each monomer of the pentamer by that of glycine, lysine or glutamine to obtain the Arctic (E22G), Italian (E22K), and Dutch (E22Q) mutants. The structure of the E22Δ-Aβ-amyloid deletion mutant was obtained by homology modelling with MODELLER6.2 [29] using the wildtype pentamer as template. All structures were N-terminally acetylated using SYBYL7.3 followed by 100 steps of conjugate gradient minimisation to release bad contacts.

Molecular dynamics simulations

All MD simulations were performed by using the AMBER9 [30] suite of programs with the force field ff99SB [31], which augments the united parameter sets of ff94 [32] and ff99 [33, 34] with updated torsion potentials. The systems were neutralised by the addition of an appropriate number of sodium or chloride counter ions. Subsequently, the molecules were solvated in a water box using the TIP3P water model [35].

Minimisation and MD were carried out using the SANDER module of AMBER9 with default settings for non-bonded interactions. Particle mesh Ewald (PME) summation [36] was used to calculate the long-range electrostatic interactions. Minimisation was carried out in two subsequent steps. In a first step, only water molecules were minimised while restraining all protein atoms on their initial positions with a force constant of 5,000 kcal mol^{-1} A^{-2}. In the second step, additional relaxation of counter ions and protons was allowed by

restraining all heavy atoms of the protein with a force constant of 50 kcal mol^{-1} A^{-2}. In both minimisations, 250 steps of steepest descent were followed by 250 steps of conjugate gradient minimisation.

MD simulations were carried out thereafter using a time step of 1 fs and periodic boundary conditions. The SHAKE procedure [37] was applied to fix all bonds involving hydrogen atoms. The temperature of the system was gradually raised from 10 K to 300 K in two subsequent equilibration steps of 0.5 and 2.5 ns. Restraints were set in both equilibration steps. In step one all protein backbone and side chain heavy atoms were fixed while in step two all backbone heavy atoms were kept in their initial positions. In the following, an unconstrained 20 ns production phase with standard NPT conditions at 1 bar was performed for data collection, saving coordinates every 1 ps to produce a total of 20,500 snapshots (including equilibration). Hierarchical clustering [38] of the 20,000 snapshots obtained during the production phase was performed using the ptraj program of AMBER10 [39]. Results were analysed and visualised using the programs AMBER, SYBYL7.3 [28], VMD [40], and DS ViewerPro 6 [41].

Energetic analysis

Since the pentameric system contains multiple protein–protein interfaces, energetic analysis requires the definition of a suitable interface. Because the present study aimed to assess the internal stability of the Aβ-pentamer, we measured the interaction energy between the middle chain C and the remaining four chains (A–B, D–E) of the pentamer (Fig. 2). The respective interaction energy represents the strength by which the middle chain clamps the Aβ-stack together and was therefore termed ΔG_{clamp}. The interaction free energy ΔG_{clamp} for the central Aβ-layer was calculated according to the standard molecular mechanical and generalised Born/surface accessible (MM/GBSA) approach [42]:

$$\Delta G_{clamp} = \Delta G_{MM} + \Delta G_{sol} - T\Delta S \quad (1)$$

ΔG_{MM} is the molecular mechanics energy for the interaction between the ligand and the receptor, and ΔG_{sol} is the solvation free energy. $-T\Delta S$ is the entropic contribution, which was estimated from normal mode analysis using the NMODE program of AMBER. ΔG_{MM} is calculated according to Eq. 2,

$$\Delta G_{MM} = \Delta G_{\mathrm{int}}^{ele} + \Delta G_{\mathrm{int}}^{vdw} \quad (2)$$

whereas the electrostatic and van der Waals interaction energies, $\Delta G_{\mathrm{int}}^{ele}$ and $\Delta G_{\mathrm{int}}^{vdw}$, were calculated with the AMBER module SANDER. Likewise, the solvation free energy ΔG_{sol}, is composed of an electrostatic $\left(\Delta G_{sol}^{ele}\right)$ and a nonpolar $\left(\Delta G_{sol}^{nonpolar}\right)$ energy term (Eq. 3)

$$\Delta G_{sol} = \Delta G_{sol}^{ele} + \Delta G_{sol}^{nonpolar} \quad (3)$$

The electrostatic contribution $\left(\Delta G_{sol}^{ele}\right)$ was calculated using the generalised born (GB) method implemented in SANDER, while nonpolar contributions to the solvation free energy $\left(\Delta G_{sol}^{nonpolar}\right)$ were calculated as a function of the solvent accessible surface area (SASA) [43] using AMBER9 default parameters for γ and b [30] (Eq. 4).

$$\Delta G_{sol}^{nonpolar} = \gamma \times SA + b \quad (4)$$

The contributions of individual side chains to pentamer stability were estimated from an in silico alanine scan, in which the amino acids of chain C were individually replaced by alanine. For the calculation of $\Delta\Delta G$, we followed the standard protocol described by Massova and Kollman [44], which assumes that the entropy of the alanine mutant and the wild type do not differ significantly, and therefore entropic contributions can be omitted for the calculation of $\Delta\Delta G$ in this type of analysis. Alanine scanning and MM/GBSA analysis for wild type Aβ-amyloid and all mutants was performed on a total of 91 pdb structures taken from the trajectory during 2.5–20.5 ns simulation time by selecting every 200th snapshot.

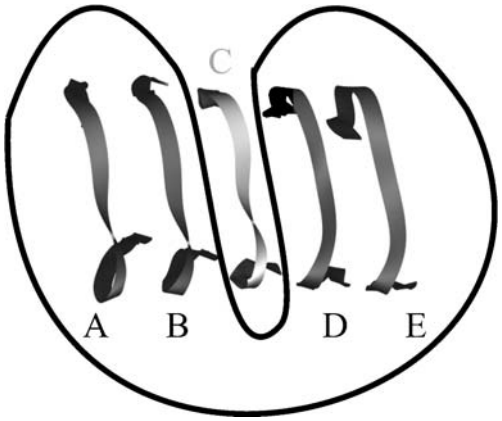

Fig. 2 Schematic drawing of the setup used for estimating the internal stability of the wild type and mutant pentamers. Free energies of interaction were calculated between the middle chain *C* (grey) and the remaining four chains (*A–B*, *D–E*) of the pentamer, thus reflecting the strength by which chain *C* clamps the Aβ stack together

Results and discussion

Mutant $A\beta_{42}$ oligomers are more rigid than the wild type

Wild type Aβ exhibits root mean square deviations (RMSD) from the starting structure of 6–8 Å (Fig. 3).

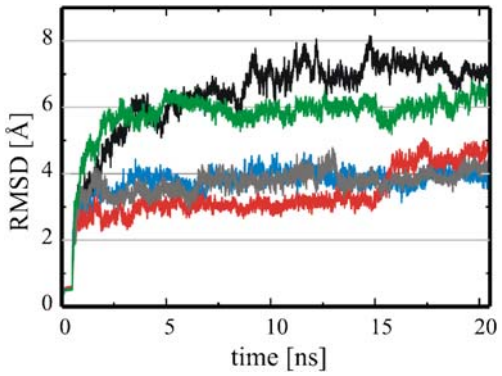

Fig. 3 Conformational stability of wild type and mutant Aβ-pentamers. *Black* Wild type, *grey* E22G, *blue* E22K, *green* E22Q, *red* E22Δ. The root mean square deviation (RMSD) was measured to the corresponding initial structure in each system

The magnitude of these fluctuations is consistent with the findings of a previous Aβ simulation, which obtained very similar RMSD values for the Aβ-pentamer [13]. Interestingly, all mutants investigated in the present study exhibit smaller RMSD values than the wild type. The highest conformational stability is observed for mutants E22G, E22K, and E22Δ, which show RMSD values of less than 4 Å for most parts of the simulation.

This finding also indicates that the high RMSD detected for the wild type can be attributed more to particular sequence properties of the wild type than to inaccuracies of the starting model. If the starting structure were inaccurate, large RMSD values would be expected for all simulations. In contrast, the present study reveals that the conformational stability of Aβ oligomers is highly dependent on the identity of the amino acid at sequence position 22.

Visual inspection of the trajectories together with RMSD profiles and the structures produced over the trajectory (Fig. 4) proved that the overall Aβ structure was stable in all simulations. The U-shaped arrangement of the two stacked parallel β-sheets and the intermolecular D23/K28 salt bridges are preserved in all simulations. The higher RMSD values detected for the wild type and the E22Q mutant originate mainly from a larger twist of the β-sheets (Fig. 4). The presence of a twist is consistent with experimental data obtained from electron micrographs of Aβ fibrils [9] and might represent a prerequisite for the incorporation of oligomers into fibrils.

Special structural properties of the E22Δ mutant

At first glance, the observation that the overall fibril geometry is retained even after deletion of E22, and that this mutant is even more stable than the wild type might be surprising. Therefore, the effect of the E22 deletion

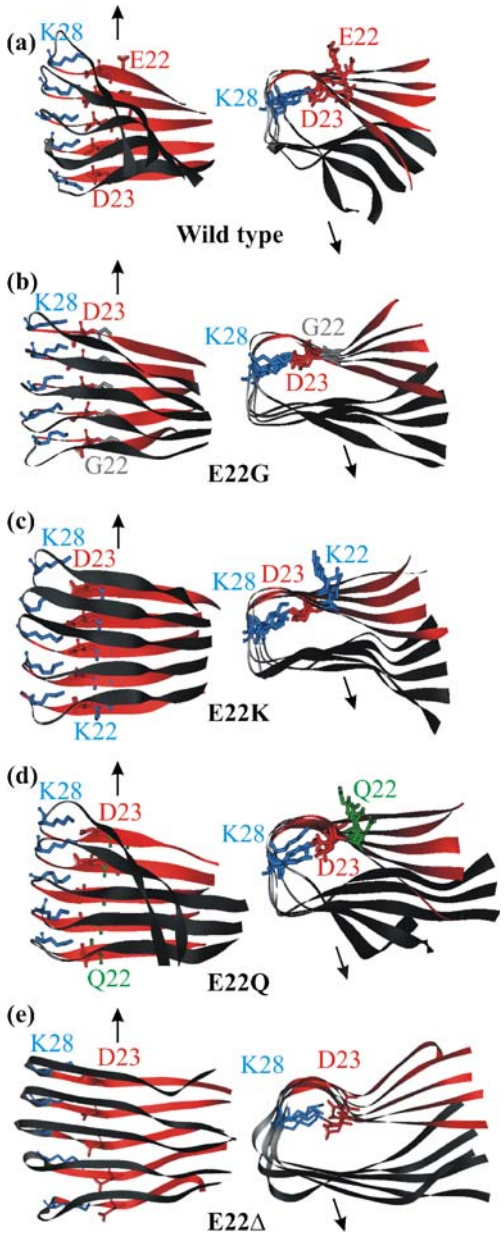

Fig. 4 Side and top view of representative structures of wild type and mutant Aβ pentamers. **a** Wild type, **b** E22G, **c** E22K, **d** E22Q, **e** E22Δ. *Red* Sheet β1, *black* sheet β2, *grey* loop. The salt bridge forming residues D23 and K28 are indicated. *Arrows* point towards growth direction with chain A on the growing end

on the backbone geometry was analysed in more detail. Significant differences in backbone torsion angles between wild type and E22Δ were observed only for the three residues C-terminally adjacent to the site of deletion (Fig. 5). D23 adopts a turn structure in the mutant instead of an extended conformation in the wild type. A very similar change from an extended conformation in the wild type to a turn structure is also observed for G25, while the V24 backbone undergoes only smaller changes.

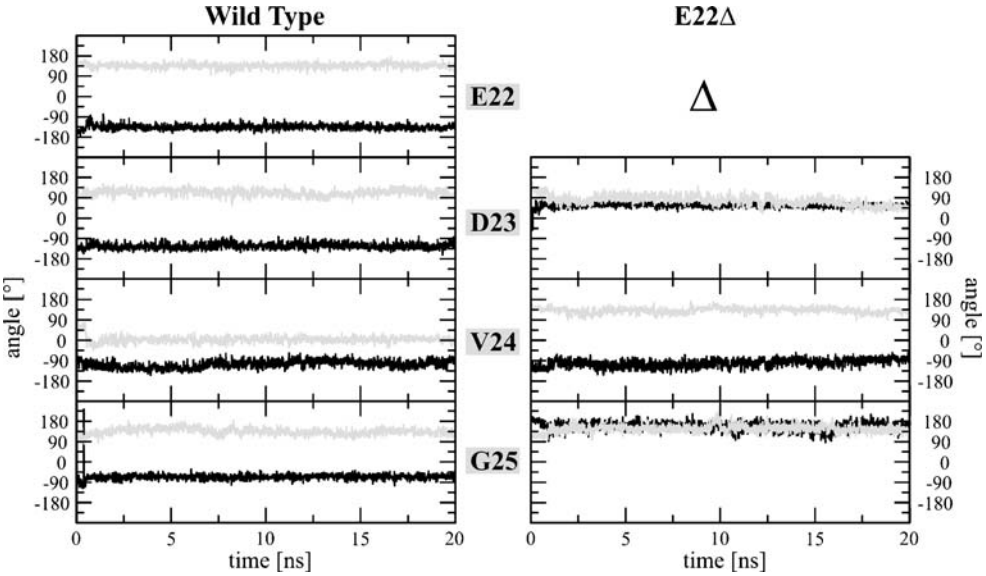

Fig. 5 Dihedral angles of residues E22 to G25 of chain C as a function of simulation time. *Left panel* Angles for the wild type, *right panel* angles for the E22Δ variant. *Black* ϕ angle (C_{i-1}–N_i–C_i^{α}–C_i), *grey* ψ angle (N_i–C_i^{α}–C_i–N_{i+1}). Δ indicates deleted residue E22

Taken together, these changes lead to an alternative backbone conformation of residues D23–V25 in E22Δ, while the backbone conformation of the remaining residues is not significantly affected by the mutation. The backbone topology of E22Δ is stable over the entire simulation time and shows only minor fluctuations (Fig. 5). Importantly, this conformation also allows for preservation of the inter-chain D23–K28 salt bridge in the mutant (Figs. 4e, 6), which was described previously as playing a crucial role in pentamer stability [9].

The observation that the sequence region that connects both β-strands exhibits a certain degree of variability is also consistent with previous studies. The models derived thus far for $A\beta_{40}$ [7, 8, 10, 45] and $A\beta_{42}$ [9] filaments consistently show two β-strands and a buried D23–K28 salt bridge that stabilises the connecting turn. The exact length and geometry of the turn, however, varies between these models. These findings suggest that Aβ exhibits a particular conformational plasticity in this region, which not only allows the formation of distinct turn geometries, but even tolerates the deletion of one residue.

Energetic analysis indicates a destabilising effect of E22

The RMSD values obtained over the MD simulations (Fig. 3) reveal the higher conformational stability of mutant $A\beta_{42}$ oligomers compared to the wild type. As the five pentamers differ solely by the amino acid at position 22, this residue appears to be the crucial determinant for stability in the investigated systems.

An alanine scan revealed a similar profile for the wild type and mutants (Fig. 7a). This indicates that the role of the individual side chains in overall stabilisation is comparable in all pentamers investigated. This is consistent with the fact that the overall Aβ-fold is preserved in all simulations (Fig. 4). The alanine scan also revealed those side chains that play a particularly important role: residues D23 and K28, which form inter-chain salt bridges, as well as the hydrophobic residues L17, F19 and F20 are the main contributors to internal stability of the $A\beta_{42}$ oligomer (Fig. 7a). Analysis of wild type $A\beta_{42}$ (Fig. 7a; black bars) further reveals that all side chains except E22 exert a stabilising effect on the pentamer fold. This is reflected by positive ΔΔG values indicating that

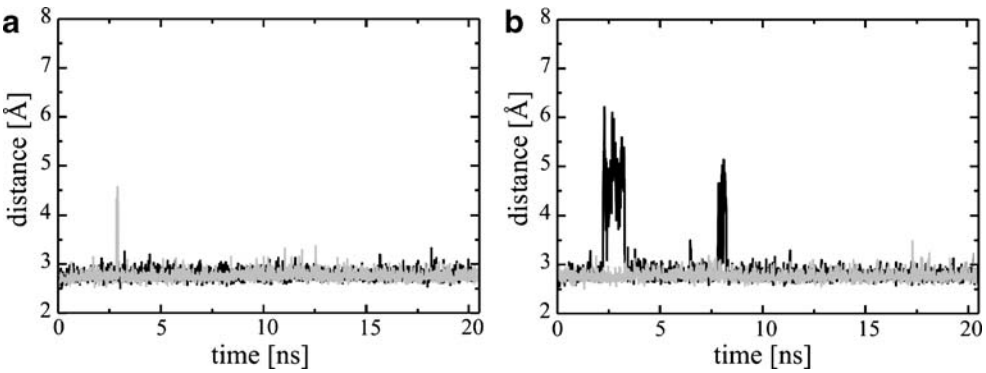

Fig. 6 Salt bridges formed by D23 and K28 of chain C in the wildtype (*black*) and mutant (*grey*). **a** Interaction between K28 of chain C and D23 of chain B. **b** Interaction between D23 of chain C and K28 of chain D

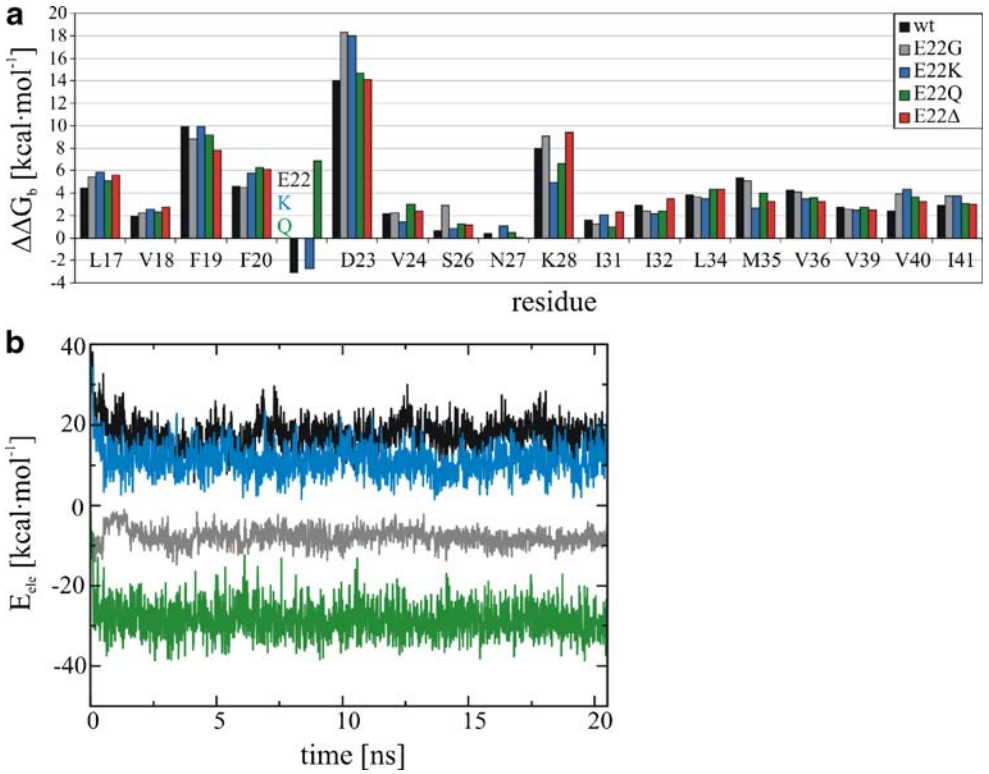

Fig. 7 Energetic analysis of Aβ-mutants. **a** Alanine scanning of wild type and E22-Aβ_{42} mutants. The contributions of individual side chains to the interaction free energy ($\Delta\Delta G_{clamp}$) of chain C to the adjacent four chains of the pentamer are shown. Positive values indicate a stabilising effect of the respective amino acid compared to alanine. No scan was performed for alanine and glycine. **b** Electrostatic interaction energy (E_{ele}) of residue 22 of chain C relative to the adjacent four chains (A–B, D–E) as a function of simulation time. *Black* Wild type, *grey* E22G, *blue* E22K, *green* E22Q

replacement of the respective side chain would weaken the interactions with adjacent chains in the wild type pentamer. E22, which represents the site of mutation, evidently plays a unique role, since the glutamate present in the wild type leads to a destabilisation of approximately 3 kcal mol^{-1} compared to an uncharged alanine. The structural explanation for this destabilising effect comes from the arrangement of the Aβ-stack as a parallel β-sheet, which places the negatively charged E22 side chains of adjacent layers in immediate vicinity to each other (see Fig. 1a).

Mutations that change E22 to a uncharged residue are therefore expected to abrogate repulsion between adjacent Aβ-chains and to result in stabilisation of the pentamer. Such a situation occurs with the E22G and E22Q mutants. While no alanine scan can be performed for position 22 in E22G due to the simulation setup, the stabilising effect of G22 and Q22 can clearly be seen from the plot of the electrostatic interaction energy shown in Fig. 7b. It is also interesting to note that electrostatic repulsion is less severe for E22K compared to the wild type (Fig. 7a, b). This finding can most likely be

Table 2 Interaction energies (in kcal mol^{-1}) of the middle chain C with the remaining four chains of the Aβ-pentamer. Values were calculated for the wild type, E22G, E22K, E22Q, and E22Δ using the molecular mechanical and generalised Born/surface accessible (MM/GBSA) strategy (see Materials and methods for details). Differences in interaction energies ($\Delta\Delta G_{clamp}$) were obtained using the wild type ΔG_{clamp} value as reference

	ΔG_{int}^{ele}	Δ_{int}^{vdw}	ΔG_{sol}^{ele}	$\Delta G_{sol}^{nonpolar}$	ΔG_{sol}	$T\Delta S$	ΔG_{clamp}	$\Delta\Delta G_{clamp}$
Wildtype	−4.4±0.3	−239.1±0.2	+64.3±0.3	−33.7±0.0	+30.5±0.3	−80.6	−132.4	–
E22G	−191.7±0.4	−246.9±0.1	+232.3±0.3	−35.4±0.0	+196.9±0.3	−83.8	−158.0	−25.6
E22K	+37.1±0.3	−245.3±0.1	+12.3±0.3	−34.6±0.0	−22.4±0.3	−90.2	−140.4	−8.0
E22Q	−193.8±0.4	−250.8±0.1	+237.1±0.3	−34.2±0.0	+202.9±0.3	−83.2	−158.5	−26.1
E22Δ	−208.0±0.4	−241.9±0.1	+243.7±0.3	−34.4±0.0	+209.3±0.3	−83.3	−157.3	−24.9

explained by the fact that the longer K22 side chain has greater conformational freedom and can therefore adopt alternative conformations that more efficiently reduce the repulsion of adjacent Aβ-layers.

In order to quantify the effect of the E22 mutation, the stability of the stack was estimated from calculating the free energies of stabilisation (ΔG_{clamp}) for the middle Aβ-chain from a MM/GBSA analysis (see Materials and methods for details). The respective interaction energy represents the strength by which the middle chain clamps the Aβ-stack together and was therefore used as a measure of the internal stability of the pentamer.

The negative $\Delta\Delta G_{clamp}$ values of −8.0 to −26.1 kcal mol^{-1} indicate that all mutant Aβ-pentamers exhibit a higher internal stability than the wild type (Table 2). In addition, the analyses demonstrate that not only mutation of E22, but also the complete deletion of this residue results in enhanced pentamer stability. Oligomers with a deleted residue E22 or an E22G/Q point mutation show higher internal stability compared to the E22K mutation (Table 2), indicating a higher oligomerisation tendency. This is in accordance with previous experimental studies, from which there are several lines of evidence for E22G and E22Q forming nonfibrillar toxic assemblies, while for E22K generally lower toxicity and aggregation potency are reported [22, 46–49]. In addition, our observations match the stated correlation between hydrophobicity and charge at position 22 and aggregation rate of Aβ-amyloid, which describes an increased aggregation rate with gaining hydrophobicity [50]. Thus, the observed lower aggregation tendency of E22K fits this correlation.

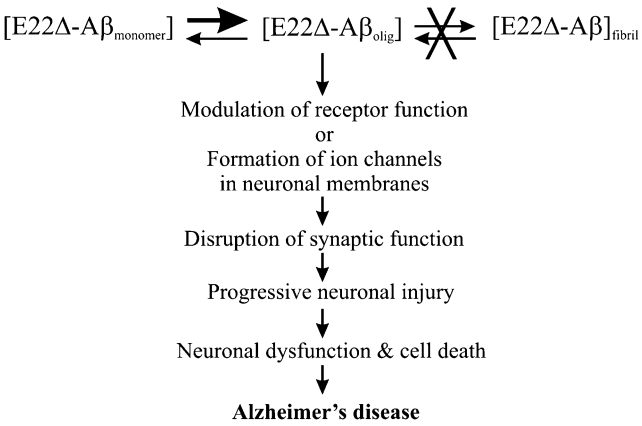

Fig. 8 Schematic representation showing the effects of E22 deletion (or mutation) on Aβ-aggregation. Firstly, the higher internal stability of the mutant oligomers increases the rate of oligomer formation and stability (*thick arrow*). Secondly, the altered dynamics and surface properties hamper fibril formation (*black cross*), thus additionally contributing to the enrichment of oligomers (see text for details). These oligomers trigger a cascade of events leading to Alzheimer's disease

Effects of E22 mutation on fibril formation

The data above offers a structural explanation for the experimental observation that the lack of a glutamate at position 22 facilitates the formation of stable oligomers. In addition to enhanced oligomer stability, the mutants also exhibit a hampered formation of fibrils as a second common property (Table 1). The impeded fibrillation of mutant Aβ was investigated computationally in a previous study [13] and has been attributed mainly to the lack of stabilising interactions within the lateral interface, such as the loss of the intermolecular E22–K16 salt bridge (Fig. 1d). A second effect on fibril formation, which emerges from our study, might result from the altered dynamics of the mutant pentamers: it is known from electron microscopic data [51] that fibrils are twisted significantly along their axis. Such twisting requires a certain degree of internal flexibility of the two β-sheets against each other. Our simulations revealed that the wild type has a high internal flexibility (Fig. 3) and that twisting is less pronounced in the mutants (Fig. 4). This effect should generally hamper the lateral association of mutant Aβ, regardless of the interface involved. In this context, the finding that the E22Δ variant exhibits a particularly rigid structure (Fig. 3), also offers an explanation for the experimental observation that this mutant shows a complete lack of fibrillation [23].

Conclusions

The findings above suggest that there are at least two structural effects of mutations at position 22 of Aβ (Fig. 8). Firstly, the mutant oligomers themselves exhibit a higher internal stability due to the lack of electrostatic repulsion between adjacent E22 residues. Secondly, the mutant oligomers can no longer be incorporated into fibrils. Together, both effects suggest a mechanism for the enrichment and enhanced stability of Aβ-oligomers observed in experimental studies (Table 1).

This dual effect of E22 mutations offers an explanation of why changes at this sequence position have such a drastic effect on progression of the disease. Finally, these findings affirm the oligomer hypothesis of AD, which claims prefibrillar aggregates and oligomers to be direct effectors of synaptic and cognitive dysfunction in AD (Fig. 8). The correlation between internal stability, aggregation tendency, and pathogenicity might also be helpful for the design of drugs targeting small but toxic Aβ-amyloid compounds.

Acknowledgements The authors thank the High Performance Computing group of the Regionales Rechenzentrum Erlangen for providing AMBER executables optimised for parallel execution. This work was funded by the Volkswagen Foundation.

References

1. Alzheimer A (1907) Über eine eigenartige Erkrankung der Hirnrinde. Allg Z Psychiat Psych-Gerichtl Med 64:146–148
2. Siegel G, Albers RW, Brady S, Price D (2005) Basic Neurochemistry, 7th edn. Elsevier, Amsterdam
3. Brun A, Englund E (1981) Regional pattern of degeneration in Alzheimer's disease: neuronal loss and histopathological grading. Histopathology 5:549–564
4. Morris JC, Price AL (2001) Pathologic correlates of nondemented aging, mild cognitive impairment, and early-stage Alzheimer's disease. J Mol Neurosci 17:101–118
5. Irie K, Murakami K, Masuda Y, Morimoto A, Ohigashi H, Ohashi R, Takegoshi K, Nagao M, Shimizu T, Shirasawa T (2005) Structure of beta-amyloid fibrils and its relevance to their neurotoxicity: implications for the pathogenesis of Alzheimer's disease. J Biosci Bioeng 99:437–447
6. Finder VH, Glockshuber R (2007) Amyloid-beta aggregation. Neurodegener Dis 4:13–27
7. Petkova AT, Ishii Y, Balbach JJ, Antzutkin ON, Leapman RD, Delaglio F, Tycko R (2002) A structural model for Alzheimer's beta-amyloid fibrils based on experimental constraints from solid state NMR. Proc Natl Acad Sci USA 99:16742–16747
8. Petkova AT, Yau WM, Tycko R (2006) Experimental constraints on quaternary structure in Alzheimer's beta-amyloid fibrils. Biochemistry 45:498–512
9. Lührs T, Ritter C, Adrian M, Riek-Loher D, Bohrmann B, Dobeli H, Schubert D, Riek R (2005) 3D structure of Alzheimer's amyloid-beta (1–42) fibrils. Proc Natl Acad Sci USA 102:17342–17347
10. Ma B, Nussinov R (2006) Simulations as analytical tools to understand protein aggregation and predict amyloid conformation. Curr Opin Chem Biol 10:445–452
11. Sato T, Kienlen-Campard P, Ahmed M, Liu W, Li H, Elliott JI, Aimoto S, Constantinescu SN, Octave JN, Smith SO (2006) Inhibitors of amyloid toxicity based on beta-sheet packing of Abeta40 and Abeta42. Biochemistry 45:5503–5516
12. Fawzi NL, Kohlstedt KL, Okabe Y, Head-Gordon T (2008) Protofibril assemblies of the arctic, Dutch, and Flemish mutants of the Alzheimer's Abeta1–40 peptide. Biophys J 94:2007–2016
13. Zheng J, Jang H, Ma B, Tsai CJ, Nussinov R (2007) Modeling the Alzheimer Abeta17–42 fibril architecture: tight intermolecular sheet-sheet association and intramolecular hydrated cavities. Biophys J 93:3046–3057
14. Zheng J, Ma B, Chang Y, Nussinov R (2008) Molecular dynamics simulations of Alzheimer Abeta40 elongation and lateral association. Front Biosci 13:3919–3930
15. Zheng J, Jang H, Ma B, Nussinov R (2008) Annular structures as intermediates in fibril formation of Alzheimer Abeta17–42. J Phys Chem B 112:6856–6865
16. Selkoe DJ (1991) The molecular pathology of Alzheimer's disease. Neuron 6:487–498
17. Hardy J, Selkoe DJ (2002) The amyloid hypothesis of Alzheimer's disease: progress and problems on the road to therapeutics. Science 297:353–356
18. McLean CA, Cherny RA, Fraser FW, Fuller SJ, Smith MJ, Beyreuther K, Bush AI, Masters CL (1999) Soluble pool of Abeta amyloid as a determinant of severity of neurodegeneration in Alzheimer's disease. Ann Neurol 46:860–866
19. Haass C, Selkoe DJ (2007) Soluble protein oligomers in neurodegeneration: lessons from the Alzheimer's amyloid beta-peptide. Nat Rev Mol Cell Biol 8:101–112
20. Caughey B, Lansbury PT (2003) Protofibrils, pores, fibrils, and neurodegeneration: separating the responsible protein aggregates from the innocent bystanders. Annu Rev Neurosci 267–298
21. Murakami K, Irie K, Morimoto A, Ohigashi H, Shindo M, Nagao M, Shimizu T, Shirasawa T (2003) Neurotoxicity and physicochemical properties of Abeta mutant peptides from cerebral amyloid angiopathy: implication for the pathogenesis of cerebral amyloid angiopathy and Alzheimer's disease. J Biol Chem 278:46179–46187
22. Nilsberth C, Westlind-Danielsson A, Eckman CB, Condron MM, Axelman K, Forsell C, Stenh C, Luthman J, Teplow DB, Younkin SG, Naslund J, Lannfelt L (2001) The 'Arctic' APP mutation (E693G) causes Alzheimer's disease by enhanced Abeta protofibril formation. Nat Neurosci 4:887–893
23. Tomiyama T, Nagata T, Shimada H, Teraoka R, Fukushima A, Kanemitsu H, Takuma H, Kuwano R, Imagawa M, Ataka S, Wada Y, Yoshioka E, Nishizaki T, Watanabe Y, Mori H (2008) A new amyloid beta variant favoring oligomerization in Alzheimer's-type dementia. Ann Neurol 63:377–387
24. Takuma H, Teraoka R, Mori H, Tomiyama T (2008) Amyloid-beta E22Delta variant induces synaptic alteration in mouse hippocampal slices. NeuroReport 19:615–619
25. Krone MG, Baumketner A, Bernstein SL, Wyttenbach T, Lazo ND, Teplow DB, Bowers MT, Shea JE (2008) Effects of familial Alzheimer's disease mutations on the folding nucleation of the amyloid beta-protein. J Mol Biol 381:221–228
26. Olofsson A, Sauer-Eriksson AE, Ohman A (2006) The solvent protection of alzheimer amyloid-beta-(1–42) fibrils as determined by solution NMR spectroscopy. J Biol Chem 281:477–483
27. Olofsson A, Sauer-Eriksson AE, Ohman A (2009) Amyloid fibril dynamics revealed by combined hydrogen/deuterium exchange and nuclear magnetic resonance. Anal Biochem 385:374–376
28. Tripos (1991–2008) Sybyl7.3. St. Louis, MO
29. Eswar N, Eramian D, Webb B, Shen MY, Sali A (2008) Protein structure modeling with MODELLER. Methods Mol Biol 145–159
30. Case DA, Darden TA, Cheatham TE, Simmerling CL, Wang J, Duke RE, Luo R, Merz KM, Pearlman DA, Crowley M, Walker RC, Zhang W, Wang B, Hayik S, Roitberg A, Seabra G, Wong KF, Paesani F, Wu X, Brozell S, Tsui V, Gohlke H, Yang L, Tan C, Mongan J, Hornak V, Cui G, Beroza P, Mathews DH, Schafmeister C, Ross WS, Kollman PA (2006) AMBER9. University of California, San Francisco, CA
31. Hornak V, Abel R, Okur A, Strockbine B, Roitberg A, Simmerling C (2006) Comparison of multiple Amber force fields and development of improved protein backbone parameters. Proteins 65:712–725
32. Cornell WD, Cieplak P, Bayly CI, Gould R, Merz KMJ, Ferguson DM, Spellmeyer DC, Fox T, Caldwell JW, Kollman PA (1995) A second generation force field for the simulation of proteins, nucleic acids and organic molecules. J Am Chem Soc 117:5179–5197
33. Cheatham TE 3rd, Cieplak P, Kollman PA (1999) A modified version of the Cornell et al. force field with improved sugar pucker phases and helical repeat. J Biomol Struct Dyn 16:845–862
34. Wang J, Cieplak P, Kollman PA (2000) How well does a restrained electrostatic potential (RESP) model perform in calculating conformational energies of organic and biological molecules? J Comput Chem 21:1049–1074
35. Jorgensen WL, Chandrasekhar J, Madura JD, Impey RW, Klein ML (1983) Comparison of simple potential functions for simulationg liquid water. J Chem Phys 79:926–935
36. Darden TA, York DM, Pedersen LG (1993) Particle Mesh Ewald. An N.log(N) method for Ewald sums in large systems. J Chem Phys 98:10089–10092
37. Ryckaert JP, Ciccotti G, Berendsen HJC (1977) J Comput Phys 23:327–341
38. Shao J, Tanner SW, Thompson N, Cheatham TE III (2007) Clustering molecular dynamics trajectories: 1. Characterizing the

performance of different clustering altorithms. J Chem Theory Comput 3:2312–2334
39. Pearlman DA, Darden TA, Cheatham TE, III, Simmerling CL, Wang J, Duke RE, Luo R, Crowley M, Walker RC, Zhang W, Merz KM, Wang B, Hayik S, Roitberg A, Seabra B, Kolossováry I, Wong KF, Paesani F, Vanicek J, Wu X, Brozell S, Steinbrecher T, Gohlke H, Yang L, Tan C, Mongan J, Hornak V, Cui G, Mathews DH, Seetin MG, Sagui C, Babin V, Kollman PA (2008) Amber 10, San Francisco, CA
40. Humphrey W, Dalke A, Schulten K (1996) VMD: visual molecular dynamics. J Mol Graph 14(33–38):27–38
41. Accelrys (2005) DS ViewerPro Suite 6.0. San Diego, CA
42. Kollman PA, Massova I, Reyes C, Kuhn B, Huo S, Chong L, Lee M, Lee T, Duan Y, Wang W, Donini O, Cieplak P, Srinivasan J, Case DA, Cheatham TE 3rd (2000) Calculating structures and free energies of complex molecules: combining molecular mechanics and continuum models. Acc Chem Res 33:889–897
43. Sitkoff D, Sharp K, Honig B (1994) Accurate calculation of hydration free energies using macroscopic sovent models. J Phys Chem 98:1978–1988
44. Massova I, Kollmann PA (1999) Computational Alanine scanning to probe protein-protein interactions: a novel approach to evaluate binding free energies. J Am Chem Soc 121:8133–8143
45. Petkova AT, Leapman RD, Guo Z, Yau WM, Mattson MP, Tycko R (2005) Self-propagating, molecular-level polymorphism in Alzheimer's beta-amyloid fibrils. Science 307:262–265
46. Whalen BM, Selkoe DJ, Hartley DM (2005) Small non-fibrillar assemblies of amyloid beta-protein bearing the Arctic mutation induce rapid neuritic degeneration. Neurobiol Dis 20:254–266
47. Miravalle L, Tokuda T, Chiarle R, Giaccone G, Bugiani O, Tagliavini F, Frangione B, Ghiso J (2000) Substitutions at codon 22 of Alzheimer's abeta peptide induce diverse conformational changes and apoptotic effects in human cerebral endothelial cells. J Biol Chem 275:27110–27116
48. Sian AK, Frears ER, El-Agnaf OM, Patel BP, Manca MF, Siligardi G, Hussain R, Austen BM (2000) Oligomerization of beta-amyloid of the Alzheimer's and the Dutch-cerebral-haemorrhage types. Biochem J 349:299–308
49. Paris D, Ait-Ghezala G, Mathura VS, Patel N, Quadros A, Laporte V, Mullan M (2005) Anti-angiogenic activity of the mutant Dutch A(beta) peptide on human brain microvascular endothelial cells. Brain Res Mol Brain Res 136:212–230
50. Päiviö A, Jarvet J, Graslund A, Lannfelt L, Westlind-Danielsson A (2004) Unique physicochemical profile of beta-amyloid peptide variant Abeta1-40E22G protofibrils: conceivable neuropathogen in arctic mutant carriers. J Mol Biol 339:145–159
51. Tycko R (2006) Molecular structure of amyloid fibrils: insights from solid-state NMR. Q Rev Biophys 39:1–55
52. Eisenhauer PB, Johnson RJ, Wells JM, Davies TA, Fine RE (2000) Toxicity of various amyloid beta peptide species in cultured human blood-brain barrier endothelial cells: increased toxicity of dutch-type mutant. J Neurosci Res 60:804–810